Atmospheric Scintillation at Dome C, Antarctica: Implications for Photometry and Astrometry

S. L. KENYON, J. S. LAWRENCE, M. C. B. ASHLEY, AND J. W. V. STOREY

School of Physics, University of New South Wales, Sydney, NSW 2052, Australia; suzanne@phys.unsw.edu.au

A. TOKOVININ

Cerro Tololo Inter-American Observatory, Casilla 603, La Serena, Chile

AND

E. FOSSAT

Laboratoire Universitaire d'Astrophysique de Nice, Université de Nice, France

ABSTRACT.   We present low-resolution turbulence profiles of the atmosphere above Dome C, Antarctica, measured with the MASS instrument during 25 nights in 2004 March–May. Except for the lowest layer, Dome C has significantly less turbulence than Cerro Tololo and Cerro Pachón. In particular, the integrated turbulence at 16 km is *always less* than the median values at the two Chilean sites. From these profiles we evaluate the photometric noise produced by scintillation, and the atmospheric contribution to the error budget in narrow-angle differential astrometry. In comparison with the two midlatitude sites in Chile, Dome C offers a potential gain of about 3.6 in both photometric precision (for long integrations) and narrow-angle astrometry precision. These gain estimates are preliminary, being computed with average wind-speed profiles, but the validity of our approach is confirmed by independent data. Although the data from Dome C cover a fairly limited time frame, they lend strong support to expectations that Dome C will offer significant advantages for photometric and astrometric studies.

1. INTRODUCTION

The potential of the Antarctic plateau for astronomy has been recognized for many years. In the early 1990s Gillingham (1991, 1993) suggested that the atmospheric turbulence above a thin boundary layer would generally be very weak. This was confirmed by the first measurements at the South Pole by Marks et al. (1999). These showed that most turbulence is found close to the surface, in this case confined to a 200 m thick layer, with very weak turbulence at high altitudes. In comparison, at most temperate sites the turbulence is strong in the tropopause and above, caused by the interactions of the jet stream with temperature gradients in the tropopause. A brief history of astrophysics in Antarctica is presented by Indermuehle et al. (2005).

Dome C, Antarctica is potentially one of the best astronomical sites in the world. As a local maximum in elevation on the plateau, Dome C enjoys very low surface wind speeds, on average 2.9 m s^{-1} (Aristidi et al. 2005).

The atmospheric turbulence at Dome C has now been studied with four different techniques: acoustic radar, MASS (a scintillation profiling technique; see below), DIMM, and microthermal sensors. An acoustic radar, or SODAR, emits sound pulses into the air and derives the strength of the atmospheric turbulence as a function of height from the intensity and delay time of the reflected sound. A DIMM, or differential image motion monitor, observes the relative motion of two images of the same star viewed through two subapertures of a small telescope. From this, the DIMM can derive the integrated atmospheric seeing. Microthermal sensors, carried aloft on a weather balloon, make an in situ measurement of the temperature fluctuations of the air as a function of height all the way to the top of the atmosphere.

SODAR measurements in the early months of 2003 by Travouillon (2005) showed that, as expected, the surface turbulent layer at Dome C was much thinner that at the South Pole. Combined MASS and SODAR measurements of the turbulence in winter 2004 gave an average seeing of 0″.27 above 30 m, with the seeing below 0″.15 for 25% of the time (Lawrence et al. 2004b). DIMM measurements in winter 2005 (Agabi et al. 2006) confirmed these results, showing an average seeing of 0″.25 above the ground layer (Agabi et al. 2006, Fig. 1*e*), and balloon microthermal measurements by the same authors imply a median seeing of 0″.36 ± 0″.19 at a height of 30 m. They also showed the existence of an intense turbulent boundary layer, finding a median seeing of 1″.9 from ground level, with 87%

924

of the total atmospheric turbulence confined to the first 36 m of atmosphere.

As expected, at Dome C the sky background in the infrared (Walden et al. 2005) is lower than at temperate sites because of the extremely cold temperatures and lower precipitable water vapor. For the same reason, the atmospheric transmission in the submillimeter is higher than at temperate sites (Calisse et al. 2004). An assessment of the optical sky brightness has been recently published by Kenyon & Storey (2006).

To date, the winter time scintillation at Dome C has only been estimated from atmospheric models (e.g., Swain et al. 2003). Scintillation is an important factor in measurements requiring high-precision photometry (e.g., extrasolar planet detection) and astrometry, and of objects with very fast intensity changes (e.g., asteroseismology; Heasley et al. 1996; Fossat 2005).

Here we evaluate the scintillation noise contribution to photometry and the atmospheric noise contribution to narrow-angle astrometry, using a set of low-resolution turbulence profiles measured at Dome C in 2004. The instrument and data are described in § 2. In § 3 we outline the theory of atmospheric turbulence, scintillation, and interferometry. In § 4 we present our results and discussion.

2. MASS MEASUREMENTS

The turbulence profile of the atmosphere at Dome C was monitored with a MASS (multiaperture scintillation sensor) instrument during the first 2 months of the 2004 night time: 2004 March 23 to 2004 May 16. The analysis of these data in terms of seeing has been reported by Lawrence et al. (2004b).

The MASS instrument and theory are described in detail in Kornilov et al. (2003) and Tokovinin et al. (2003). In brief, starlight is directed via a telescope onto four concentric annular mirrors that split the entrance aperture into rings with projected outer diameters of 19, 32, 56, and 80 mm. Each of the four beams is directed to a miniature Hamamatsu photomultiplier that samples the stellar intensity at a 1 kHz rate. Four normal and six differential scintillation indices are calculated for each 1 s integration and further averaged during 1 minute. The set of 10 indices is fitted to a model of six fixed layers at heights 0.5, 1, 2, 4, 8, and 16 km above the observatory. For each layer i, the integrated turbulence J_i (m$^{1/3}$) is calculated:

$$J_i = \int_{\text{Layer } i} C_n^2(h)dh, \qquad (1)$$

where $C_n^2(h)$ (m$^{-2/3}$) is the refractive index structure constant and h is the height above the site. The spectral response of MASS is from 400 to 550 nm with a FWHM bandwidth of 100 nm.

The profile restoration from scintillation indices is a delicate procedure, and errors may reach 10% of the total turbulence

integral. The errors are larger for the lower layers, while the two highest layers (8 and 16 km) are measured well. The second moment of the turbulence profile used in this paper is measured by MASS with high reliability, as well as lower moments. This has been demonstrated by intercomparing MASS and SCIDAR instruments (Tokovinin et al. 2005).

The Dome C MASS (Lawrence et al. 2004a), operated in the AASTINO (Automated Astrophysical Site Testing International Observatory; Lawrence et al. 2005), uses a gimbal-mounted siderostat mirror feeding a fixed 85 mm refracting telescope.

MASS instruments also operate at a number of other sites. To provide a comparison to the Dome C results, we have also included the publicly available data[1] from the Cerro Tololo and Cerro Pachón observatories in Chile. The profiles for Cerro Pachón have been discussed and modeled by Tokovinin & Travouillon (2006).

3. THEORY

3.1. Turbulence

Many astronomical measurements are limited by the Earth's atmosphere. A wave front located at height h and horizontal position vector x in the atmosphere can be described by its complex amplitude $\Psi_h(x)$ (Roddier 1981),

$$\Psi_h(x) = e^{\chi_h(x)+i\psi_h(x)}, \qquad (2)$$

where $\chi_h(x)$ is the logarithm of the amplitude and $\psi_h(x)$ is the phase of the wave.

Atmospheric turbulence introduces pure phase distortions. As the wave front propagates through the atmosphere, amplitude modulations appear as well. In the geometric optics approximation, phase perturbations act as positive or negative lenses, changing the wave front curvature and producing intensity modulation at the ground. Diffraction is also important and defines the size of the most effective atmospheric "lenses" to be of the order of the Fresnel radius,

$$r_F \approx (\lambda h)^{1/2}, \qquad (3)$$

where λ is the wavelength of light and h is the height of the turbulent layer above the observatory site. For example, if the dominant turbulence layer is at 10 km, then at 500 nm, $r_F = 7$ cm.

Dravins et al. (1997a, 1997b, 1998) present detailed discussions of stellar scintillation, including statistical distributions and temporal properties, dependence on wavelength, and effects for different telescope apertures.

3.2. Scintillation Noise

The scintillation index σ_I^2 is used as a measure of the amount of scintillation and is defined (for small intensity fluctuations) as the variance of $\Delta I / \langle I \rangle$. In the weak-scintillation regime, $\sigma_I^2 \ll 1$, the effects of all turbulence layers are additive. In this case, the scintillation index is related to the refractive index structure constant $C_n^2(h)$ by (Krause-Polstorff et al. 1993; Roddier 1981)

$$\sigma_I^2 = \int_0^\infty C_n^2(h)W(h)dh, \qquad (4)$$

where the weighting function $W(h)$ is given by

$$W(h) = 16\pi^2 0.033 \left(\frac{2\pi}{\lambda}\right)^2 \int_0^\infty |A(f)|^2 f^{-8/3} \sin^2\left(\frac{\lambda h f^2}{4\pi}\right) df. \qquad (5)$$

Here h is the height above the observatory, λ is the wavelength, f is the spatial frequency, and $|A(f)|^2$ is an aperture filtering function. This expression is valid for monochromatic light and has to be modified for wide-band radiation.

For telescope apertures with diameter $D \ll r_F$, the monochromatic scintillation index is (Roddier 1981)

$$\sigma_I^2 = 19.2\lambda^{-7/6}(\cos\gamma)^{-11/6} \int_0^\infty h^{5/6} C_n^2(h)dh, \qquad (6)$$

where γ is the zenith angle.

The scintillation index for a large circular aperture with diameter $D \gg r_F$ is

$$\sigma_I^2 = 17D^{-7/3}(\cos\gamma)^{-3} \int_0^\infty h^2 C_n^2(h)dh. \qquad (7)$$

Large apertures effectively average small-scale intensity fluctuations, so that only atmospheric lenses of the order of the aperture diameter D contribute to the flux modulation. In this case, geometric optics applies and the scintillation becomes independent of both the wavelength and the spectral bandwidth.

The above expressions are for very short timescale exposures. For exposure times that are longer than the time taken for a scintillation pattern to cross the telescope aperture [i.e., $t > (\pi D)/V_\perp$, where D the telescope diameter and $V_\perp$ the speed of the turbulence layer], the scintillation index can be calculated from (Dravins et al. 1998)

$$\sigma_I^2(t) = \int_0^\infty P(\nu)\text{sinc}^2(\pi\nu t)d\nu, \qquad (8)$$

where ν (s^{-1}) is the temporal frequency and $P(\nu)$ is the temporal power spectrum, given by Yura & McKinley (1983) and references therein as

$$P(\nu) \approx 8.27k^{2/3} \int_0^\infty \frac{C_n^2(h)h^{4/3}}{V_\perp(h)} Q(h)dh \qquad (9)$$

at the zenith, where $k = 2\pi/\lambda$ and

$$Q(h) = \int_0^\infty |A(f_x, f_y)|^2 \left[x^2 + \frac{\nu^2}{\nu_0^2(h)}\right]^{-11/6} \sin^2\left[x^2 + \frac{\nu^2}{\nu_0^2(h)}\right] dx. \qquad (10)$$

Here $f_x = \nu/V_\perp(h)$, $f_y = (2k/h)^{1/2}x$, $\nu_0(h) = (2k/h)^{1/2}V_\perp(h)$, and $A(f) = [2J_1(fD/2)]/(fD/2)$ for a circular aperture with diameter D and $f^2 = f_x^2 + f_y^2$.

For large t, Dravins et al. (1998) simplify equation (8) to

$$\sigma_I^2(t) = \frac{P(0)}{2t}. \qquad (11)$$

In the limit of large apertures $D \ll r_F$, we can replace the sine in equation (10) by its argument. By setting $\nu = 0$ and introducing a new variable $y = f_y D$, we can show that

$$P(0) \approx 21.3D^{-4/3} \int_0^\infty \frac{C_n^2(h)h^2}{V_\perp(h)} dh \qquad (12)$$

and is independent of the wavelength.

For a particular set of turbulence and wind profiles, the scintillation noise σ_I at zenith can be expressed as

$$\sigma_I = \begin{cases} S_1, & D \ll r_F, \\ S_2 D^{-7/6}, & D \gg r_F, \\ S_3 D^{-2/3} t^{-1/2}, & D \gg r_F, \ t \gg (\pi D)/V_\perp, \end{cases} \qquad (13)$$

where

$$S_1 = \left[19.2\lambda^{-7/6} \int_0^\infty h^{5/6} C_n^2(h)dh\right]^{1/2}, \qquad (14)$$

$$S_2 = \left[17.3 \int_0^\infty h^2 C_n^2(h)dh\right]^{1/2}, \qquad (15)$$

$$S_3 = \left[10.7 \int_0^\infty \frac{C_n^2(h)h^2}{V_\perp(h)} dh\right]^{1/2}. \qquad (16)$$

The scintillation error can be expressed in magnitudes as $\sigma_I(\text{mag}) = 2.5\log(\sigma_I + 1)$.

In all cases the scintillation noise is dominated by the high-altitude turbulence, more so in the case of large apertures be-

cause of the h^2 weighting. It is the large-aperture case that is generally of more relevance to astronomical photometry.

3.3. Astrometric Interferometry

The Antarctic plateau has been recognized as a potentially favorable site for interferometry because the high-altitude turbulence is very weak (Lloyd et al. 2002). In particular, high precision, very-narrow angle differential astrometry should be attainable at Dome C using long-baseline interferometry techniques. This would benefit a number of science programs, including extrasolar planet searches and the study of close binary and multiple star systems (for other examples, see Swain et al. 2003; Lloyd et al. 2002; Sozzetti 2005).

Differential astrometric measurement requires simultaneous observations of the target and reference object. To achieve this, each telescope has a dual feed to direct the beam from each star to the beam combiner (Shao & Colavita 1992). On combination of the beams, a fringe pattern is produced if the difference between the optical path lengths from each arm of the interferometer to the beam combiner is within $\lambda^2/\Delta\lambda$ (Lane & Muterspaugh 2004). The difference between the fringe positions of the two stars is measured. Phase referencing can be used to improve the limiting magnitude of the interferometer if the target star and reference object are within the isoplanatic patch (Shao & Colavita 1992).

Uncertainties in astrometric position measurements arise from instrumental effects (noise, systematic) and atmospheric effects associated with temporal incoherence and anisoplanatism. See Shao & Colavita (1992), Sozzetti (2005), and Lane & Muterspaugh (2004) for further details.

The variance in an astrometric position measurement caused by anisoplanatism (assuming a Kolmogorov turbulence spectrum) is described by Shao & Colavita (1992) as

$$\sigma_{\text{atm}}^2 \approx 5.25 t^{-1} \begin{cases} \theta^2 B^{-4/3} \displaystyle\int_0^\infty \frac{C_n^2(h)h^2}{V(h)}\,dh & \text{(case 1)}, \\[2ex] \theta^{2/3} \displaystyle\int_0^\infty \frac{C_n^2(h)h^{2/3}}{V(h)}\,dh & \text{(case 2)}, \end{cases} \tag{17}$$

where t is the integration time, θ is the angular separation between two stars, $C_n^2(h)$ and $V(h)$ are the vertical turbulence and wind profiles, h is the height above the site, and B is the baseline or diameter of the entrance pupil. These formulae are only approximate, but the exact coefficient is not needed for the purpose of site intercomparison.

Case 1 applies to interferometry when the integration time $t \gg B/\overline{V}$ and $\theta\overline{h} \ll B$, where $\overline{h}$ and $\overline{V}$ are the turbulence-weighted effective atmospheric height and wind speed. Because of the h^2 weighting, σ_{atm} in this regime is very sensitive to high-altitude turbulence.

Case 2 is applicable to single-dish astrometry and is independent of the size of the telescope when $\theta\overline{h} \gg B$ and $t \gg \theta\overline{h}/\overline{V}$.

For a particular set of turbulence and wind profiles, the error σ_{atm} (arcseconds) can be expressed as

$$\sigma_{\text{atm}} = \begin{cases} C_1 t^{-1/2}\theta B^{-2/3} & \text{(case 1)}, \\ C_2 t^{-1/2}\theta^{1/3} & \text{(case 2)}, \end{cases} \tag{18}$$

where

$$C_1 = 472{,}000 \left[\int_0^\infty \frac{C_n^2(h)h^2}{V(h)}\,dh\right]^{1/2} \tag{19}$$

and

$$C_2 = 472{,}000 \left[\int_0^\infty \frac{C_n^2(h)h^{2/3}}{V(h)}\,dh\right]^{1/2}. \tag{20}$$

Note that the expression for C_1 contains the same combination of atmospheric parameters as the expression for the photometric error S_3. This is not a coincidence, as both narrow-angle astrometry and large-aperture photometry are affected by the same physical phenomenon: large-scale curvature fluctuations of wave fronts. Hence, scintillation in large apertures contains information on the potential accuracy of narrow-angle astrometry at a given site.

4. RESULTS

Using the eight weeks of MASS data from Dome C, we extracted 11,532 turbulence profiles spread over 51 nights (we use "night" to mean the period within 24 hr when the Sun is farther than 10° below the horizon). These data were filtered according to the criteria $B_D/F_D < 0.03$, $F_D > F_{\text{limit}}$, $\delta F_D < 0.003$, $0.7 < F_C/F_D < 0.9$, and $\chi^2 < 100$, where F_D and B_D are the star flux and background measurements in aperture D (largest aperture). Here F_{limit} is a cutoff flux limit set to 100 counts for α Trianguli and 200 counts for β Crucis and β Carinae. The parameter δF_D shows slow flux variations, used here to eliminate data affected by the guiding errors. The flux ratio F_C/F_D serves to control the aperture vignetting by the entrance window, which was sometimes covered by snow or frost. The χ^2 is a measure of the fit quality. After filtering, 1853 profiles over 26 nights remained for further analysis.

Each profile includes the integrated turbulence J_i (see eq. [1]) in layers centered at elevations of 0.5, 1, 2, 4, 8, and 16 km above the site with vertical resolution $\Delta h/h \sim 0.5$. Finally, we calculated the scintillation noise and implied astrometric error from each profile. In this section, we compare these results with similar data for the Cerro Tololo and Cerro Pachón observatories in Chile (see Table 1 for information on each data set).

Site	Location[a]	Altitude (m)	Date Range	Number of Nights	Number of Profiles
Dome C	123 21 E, 75 06 S	3260	2005 Mar 23–2004 May 16	26	1853
Cerro Tololo	70 48 W, 30 09 S	2215	2002 Mar 19–2006 Feb 2	573	98887
Cerro Pachón	70 44 W, 30 14 S	2738	2003 Jan 9–2006 Jan 30	293	39819

NOTE.—We use "night" to mean the period within 24 hr when the Sun is farther than 10° below the horizon.

[a] Location is given in degrees and arcminutes.

4.1. Turbulence Profiles

Figure 1 shows the cumulative probability that the integrated turbulence for each height is less than the given J_i.

Cerro Tololo has the lowest turbulence in the 0.5 km layer. At 1 km the turbulence at Dome C is so low that, for most of the time, it cannot be reliably measured with MASS. Dome C has a slightly higher probability of smaller turbulence in the 4 and 8 km layers. However, the most significant difference between the sites is in the 16 km layer; at Dome C the integrated turbulence in this high-altitude layer is *always less* than the median values at Cerro Tololo and Cerro Pachón.

The Cerro Tololo and Cerro Pachón sites are only 10 km apart and have a 400 m altitude difference. Hence, we expect identical high-altitude turbulence for those sites. The differences seen in Figure 1 reflect mostly different seasonal coverage of the data sets (more winter-spring data for Cerro Tololo) coupled to the systematic seasonal trends in high-altitude turbulence. Similar caution is warranted for the Dome C data that cover only 25 nights.

4.2. Wind Profiles

The photometric error for long integration times (eqs. [13] and [16]) and the astrometric errors (eqs. [19] and [20]) depend not only on the turbulence but also on the wind speed profile. As these quantities are likely correlated, the correct way to estimate the errors requires simultaneous data on wind and turbulence. The wind profiles can, in principle, be retrieved from the global meteorological databases like NCEP (National Centers for Environmental Prediction). However, here we adopt a simplified approach and use fixed wind profile models instead. Hence, the distributions derived here may be not realistic.

Owing to the strong h^2 weighting, the astrometric and photometric errors are almost entirely determined by the highest MASS layer at 16 km. Hence, the adopted wind speed in this layer critically influences our results.

The wind speed profiles for Cerro Pachón and Cerro Tololo were modeled using a constant ground layer speed V_g plus a Gaussian function to represent the jet stream contribution (Greenwood 1977):

$$V(h) = V_g + V_t \exp\left[-\left(\frac{h-H}{T}\right)^2\right], \qquad (21)$$

where h is the altitude above the observatory. We set $V_g = 8$ m s^{-1}, $V_t = 30$ m s^{-1}, $H = 8$ km, and $T = 4$ km by comparing the model to the Cerro Pachón wind profiles in Avila et al. (2000, 2001).

The summer wind speed profile at Dome C also shows a Gaussian peak at the (somewhat lower) tropopause layer (~5 km) and fairly constant wind speed at other elevations (see Fig. 4 of Aristidi et al. 2005). In the winter, the wind speed profile is different, showing an increase in stratospheric wind speeds and no peak at the tropopause. So far only three profiles of the winter wind speed have been published (Agabi et al. 2006). Figure 2 shows the average wintertime and summertime wind profiles; we used the wintertime wind profile in this work.

4.3. Scintillation Noise

The scintillation noise was calculated for the three regimes discussed in § 3.2, using the results from each site. Figure 3 shows the cumulative probabilities for S_1, S_2, and S_3.

For short timescales, the median scintillation noise at Dome C is a factor of ~2 less than at Cerro Tololo and Cerro Pachón, in the small-aperture regime. For larger apertures the gain is slightly higher, ~2.4, because of the weaker high-altitude turbulence at Dome C. As an example, for a 4 m diameter telescope, the median values of the scintillation noise at each site are 1.2 mmag (Dome C), 3.2 mmag (Cerro Tololo), and 2.8 mmag (Cerro Pachón).

The more relevant figure is the scintillation noise for long exposure times. We used the wind speed models discussed above to calculate this parameter. Dome C offers a potential gain of about 3.6 in photometric precision compared to Cerro Tololo and Cerro Pachón. From the results we calculate the median photometric error expected on a 4 m telescope for $t = 60$ s to be ~53 μmag at Dome C, ~200 μmag at Cerro Tololo, and ~180 μmag at Cerro Pachón.

As a comparison, Dravins et al. (1998) measured $P(\nu)$ at La Palma using various small apertures. From their results they extrapolate $P(0) = 5 \times 10^{-6}$ s for a 4 m aperture at zenith, which gives $\sigma_t = 220$ μmag for a 60 s integration, similar to the typical values for Cerro Tololo and Cerro Pachón. Our results are also consistent with those measured at Kitt Peak and Mauna Kea by Gilliland et al. (1993).
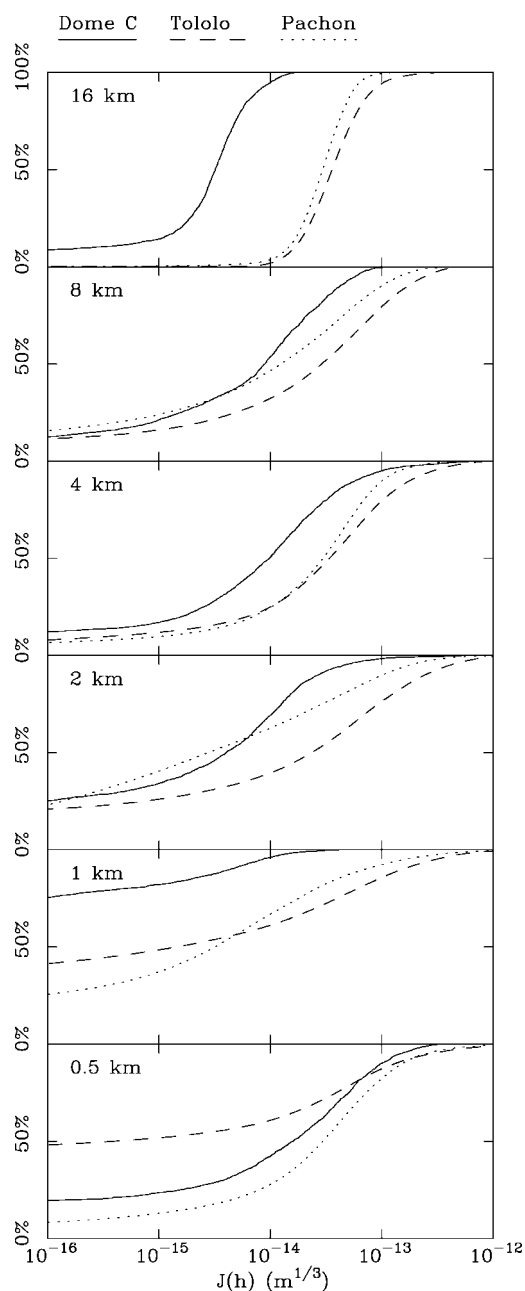
FIG. 1.—Cumulative probabilities that the integrated turbulence for each height (above the surface) is less than the given J_i for Dome C (*solid curve*), Cerro Tololo (*dashed curve*), and Cerro Pachón (*dotted curve*). The large fraction of very low J_i values for the 0.5 and 1 km layers is an artifact of the MASS profile restoration method in situations when these layers do not dominate.

4.4. Astrometry

The constants C_1 and C_2 (§ 3.3) were calculated for each site; cumulative probabilities are shown in Figure 4. The median astrometric error σ_{atm} at Dome C is ~3.5 times less than the median values at Cerro Tololo and Cerro Pachón. In Figure 5,
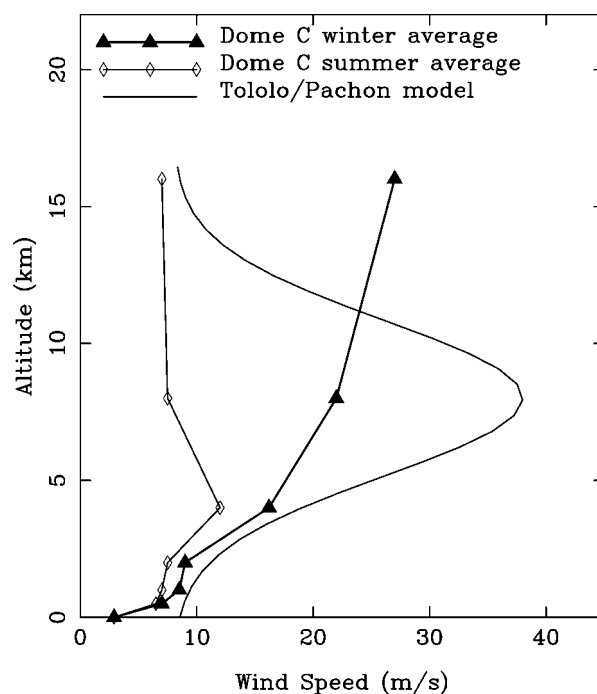
FIG. 2.—Average wind speed profiles at Dome C in the winter (Agabi et al. 2006) and summer (Aristidi et al. 2005), and a model of the wind profile at Cerro Tololo and Cerro Pachón.

σ_{atm} at Dome C is plotted for several baselines as a function of separation angle θ for an integration time of 1 hr.

We note that the advantage of Dome C for narrow-angle astrometry over midlatitude sites is even larger than its advantage in the fast scintillation. This difference is related to the adopted wind speed at 16 km altitude (27 and 8.5 m s^{-1} for Dome C and Cerro Pachón, respectively). Turbulence at Dome C is known to be slow (large time constant; see below), but the h^2 weighting in the expressions for the photometric and astrometric errors reverses this conclusion because the high-altitude turbulence dominates the calculation.

Our conclusions are conditional on the adopted wind-speed models. Using the mean Dome C winter wind speed we calculated a median C_1 value of 140 arcsec rad^{-1} m$^{2/3}$ s$^{1/2}$; decreasing the 16 km wind speed to 7 m s^{-1} gave a median C_1 value of 200 arcsec rad^{-1} m$^{2/3}$ s$^{1/2}$, still well below the median values at Cerro Tololo and Cerro Pachón. As an additional check, we computed C_1 from a set of six balloon profiles of C_n^2 and wind measured at Cerro Pachón in 1998 October (see Avila et al. 2000, 2001 for the discussion of these data). The C_1 values range from 380 to 660 arcsec rad^{-1} m^2 s$^{1/2}$, with a median of 480. This is close to the median value for Cerro Pachón given in Figure 4. Shao & Colavita (1992) calculate C_1 at Mauna Kea to be 300 arcsec rad^{-1} m^2 s$^{1/2}$, using the results from two short observing campaigns.

The fringe phase of an interferometric measurement must be determined within the atmospheric coherence time. Table 2
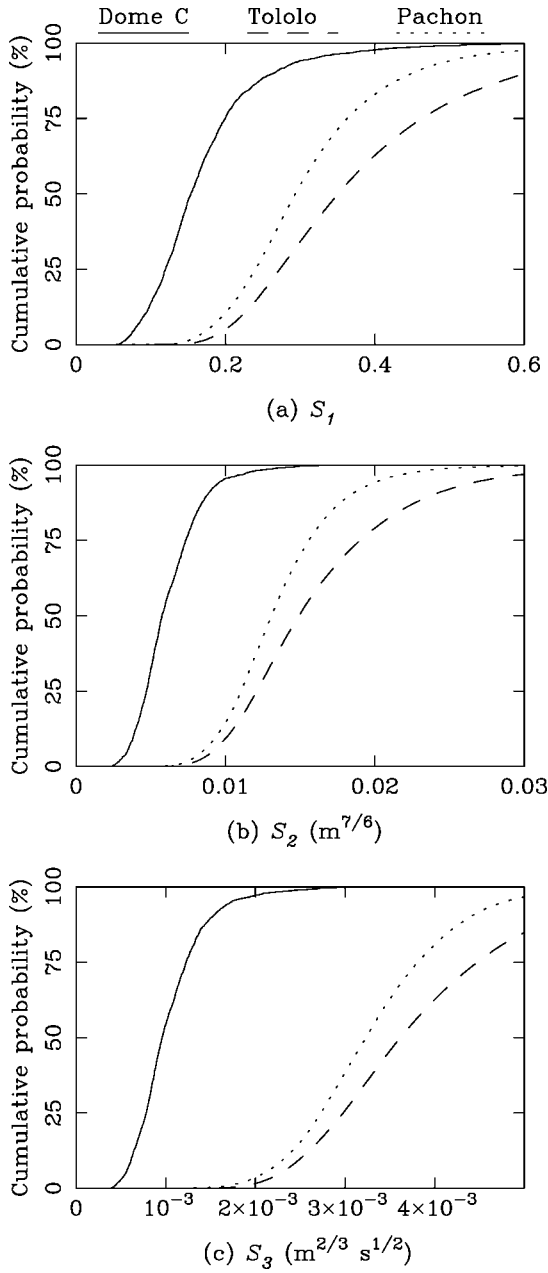
FIG. 3.—Cumulative probabilities of the constants (a) S_1, (b) S_2 (m$^{7/6}$), and (c) S_3 (m$^{2/3}$ s$^{1/2}$) for Dome C, Cerro Tololo, and Cerro Pachón. The scintillation noise σ_I is the standard deviation of $\Delta I/I$, where I is the stellar flux, and is equal to S_1 for $D \ll r_F$, $S_2 D^{-7/6}$ for $D \gg r_F$, and $S_3 D^{-2/3} t^{-1/2}$ for $D \gg r_F$ and $t \gg (\pi D)/V_\perp$, where D is the telescope diameter, r_F is radius of the Fresnel zone, and t is the integration time.

shows the median coherence times τ_0 (Roddier et al. 1982a) and isoplanatic angles θ_0 (Roddier et al. 1982b) at each site for wavelengths 500 nm and 2.2 μm. The median coherence time at Dome C, measured with MASS, is 7.2 ms at $\lambda = 500$ nm and 42 ms at $\lambda = 2.2$ μm. Using the measured turbulence
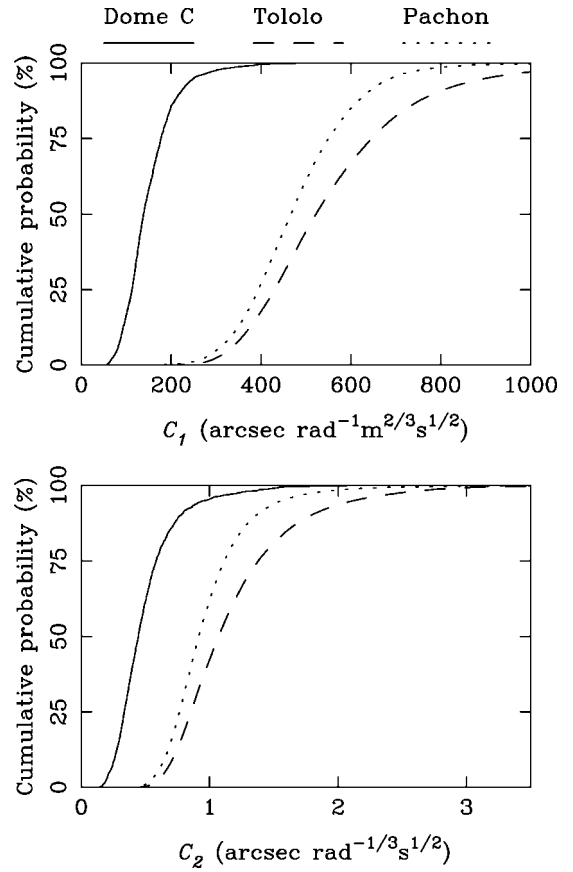
FIG. 4.—Cumulative probabilities that the constants C_1 and C_2 are less than the value given, for Dome C, Cerro Tololo, and Cerro Pachón. The astrometric error $\sigma_{\rm atm}$ (arcseconds) is equal to $C_1 t^{-1/2}\theta B^{-2/3}$ for $t \gg B/\overline{V}$ and $\theta\overline{h} \ll B$, and $C_2 t^{-1/2}\theta^{1/3}$ for $t \gg \theta\overline{h}/\overline{V}$ and $\theta\overline{h} \gg B$. Here t is the integration time, B is the baseline length, $\overline{h}$ and $\overline{V}$ are the turbulence-weighted effective atmospheric height and wind speed, and θ is the stellar separation.

profiles and assumed wind profile at Dome C, we calculated $\tau_0 = 9.4$ ms at $\lambda = 500$ nm.

Phase referencing during the measurement (Shao & Colavita 1992) effectively increases the coherence time, with the condition that the target and reference objects are within the same isoplanatic patch. The median isoplanatic angle at Dome C is ~3 times larger than at Cerro Tololo and Cerro Pachón, allowing wider fields to be used for phase referencing.

5. CONCLUSIONS

The scintillation noise at Dome C for fast exposures is typically a factor 1.9–2.6 times lower than at Cerro Tololo and Cerro Pachón, leading to a corresponding reduction in this ultimate limit for high-precision photometry. The "small aperture" scintillation index becomes important for adaptive optics when the distance between the actuators approaches the Fresnel zone size r_F and shadow patterns start becoming re-
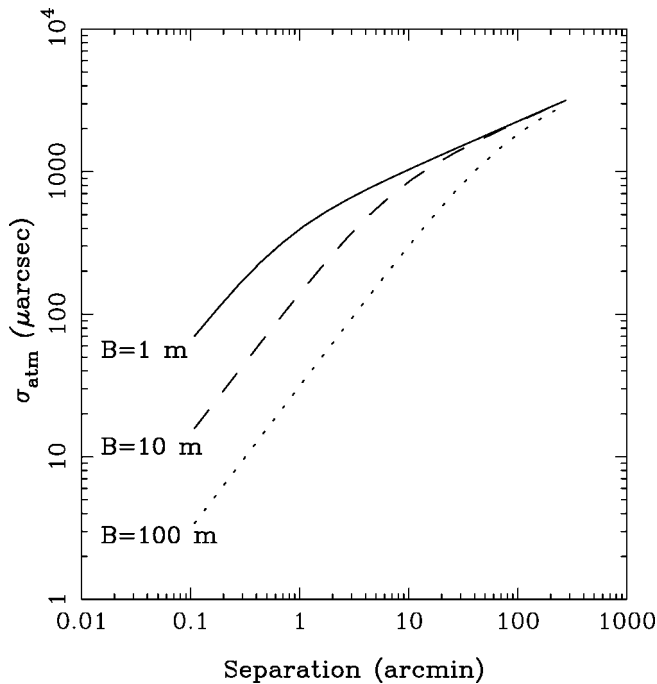
FIG. 5.—Median error σ_{atm} for three baseline lengths at Dome C, with an integration time of 1 hr.

TABLE 2
ISOPLANATIC ANGLES AND COHERENCE TIMES FOR ADAPTIVE OPTICS

Site	θ_0(500 nm) (arcsec)	τ_0(500 nm) (ms)	θ_0(2.2 μm) (arcsec)	τ_0(2.2 μm) (ms)
	Median Values			
Dome C	5.4	7.2	32	42
Cerro Tololo	1.8	2.0	11	12
Cerro Pachón	2.0	2.6	12	16
	Average Values			
Dome C	5.9	8.8	35	52
Cerro Tololo	1.9	2.8	11	17
Cerro Pachón	2.1	3.3	13	20

NOTE.—The values of τ_0 and θ_0 at 500 nm are taken from the MASS data files, and the values at 2.2 μm are scaled by $\lambda^{6/5}$.

solved (Masciadri et al. 2004). Adaptive optics will also benefit from the long coherence time and large isoplanatic angle at Dome C, particularly in the infrared.

For longer exposures, σ_I at Dome C is typically 3.4–3.8 times less than at Cerro Tololo and Cerro Pachón. For a 60 s integration on a 4 m telescope, the median photometric error is ~53 μmag at Dome C. This parameter is important for exoplanet transit measurements because the change in flux, caused by a transiting planet, is related to the planet R_p and star R_s radii by $\Delta F/F = (R_p/R_s)^2$. For example, for a Jupiter-size planet transiting a Sun-size star $\Delta F/F = 0.01$; for an Earth-size planet this ratio is 0.0001. The lower scintillation noise at Dome C will allow for the transits of smaller planets to be detected than at the Chilean sites.

The atmospheric contribution to the positional error in a differential astrometric measurement using a long-baseline interferometer at Dome C is always less than the median values at Cerro Tololo and Cerro Pachón. This conclusion is obtained

using average wind profiles and remains provisional until a more complete analysis is done.

Based on the expected low astrometric error at Dome C, a number of interferometric projects have already been proposed. These include the Antarctic Planet Interferometer (API; Swain et al. 2004), the Kiloparsec Explorer for Optical Planet Search (KEOPS; Vakili et al. 2004), and the Antarctic L-band Astrophysics Discovery Demonstrator for Interferometric Nulling (ALADDIN; Coudé du Foresto et al. 2006). Many science programs would benefit from an Antarctic interferometer, including exoplanet detection and orbit determination and measurement of microlensing events (Lloyd et al. 2002).

REFERENCES

Agabi, A., Aristidi, E., Azouit, M., Fossat, E., Martin, F., Sadibekova, T., Vernin, J., & Ziad, A. 2006, PASP, 118, 344

Aristidi, E., et al. 2005, A&A, 430, 739

Avila, R., Vernin, J., Chun, M. R., & Sanchez, L. J. 2000, Proc. SPIE, 4007, 721

Avila, R., Vernin, J., & Sánchez, L. J. 2001, A&A, 369, 364

Calisse, P. G., Ashley, M. C. B., Burton, M. G., Phillips, M. A., Storey, J. W. V., Radford, S. J. E., & Peterson, J. B. 2004, Publ. Astron. Soc. Australia, 21, 256

Coudé du Foresto, V., Absil, O., Barillot, M., & Swain, M. 2006, in IAU Colloq. 200, Direct Imaging of Exoplanets: Science and Techniques, ed. C. Aime & F. Vakili (Cambridge: Cambridge Univ. Press), 305

Dravins, D., Lindegren, L., Mezey, E., & Young, A. T. 1997a, PASP, 109, 173

———. 1997b, PASP, 109, 725

———. 1998, PASP, 110, 610

Fossat, E. 2005, in Dome C Astronomy and Astrophysics Meeting, ed. M. Giard, F. Casoli, & F. Paletou (Les Ulis: EDP Sci.), 121

Gilliland, R. L., et al. 1993, AJ, 106, 2441

Gillingham, P. R. 1991, Publ. Astron. Soc. Australia, 9, 55

———. 1993, ANARE Research Notes, No. 88, 290

Greenwood, D. P. 1977, J. Opt. Soc. Am., 67, 390

Heasley, J. N., Janes, K., Labonte, B., Guenther, D., Mickey, D., & Demarque, P. 1996, PASP, 108, 385

Indermuehle, B. T., Burton, M. G., & Maddison, S. T. 2005, Publ. Astron. Soc. Australia, 22, 73

Kenyon, S. L., & Storey, J. W. V. 2006, PASP, 118, 489

Kornilov, V., Tokovinin, A. A., Vozyakova, O., Zaitsev, A., Shatsky, N., Potanin, S. F., & Sarazin, M. S. 2003, Proc. SPIE, 4839, 837

Krause-Polstorff, J., Murphy, E. A., & Walters, D. L. 1993, Appl. Opt., 32, 4051

Lane, B. F., & Muterspaugh, M. W. 2004, ApJ, 601, 1129

Lawrence, J. S., Ashley, M. C., Kenyon, S. L., Storey, J. W. V., Tokovinin, A. A., Lloyd, J. P., & Swain, M. R. 2004a, Proc. SPIE, 5489, 174

Lawrence, J. S., Ashley, M. C., & Storey, J. W. V. 2005, J. Electrical Electron. Eng. Australia, 2, 1

Lawrence, J. S., Ashley, M. C. B., Tokovinin, A., & Travouillon, T. 2004b, Nature, 431, 278

Lloyd, J. P., Oppenheimer, B. R., & Graham, J. R. 2002, Publ. Astron. Soc. Australia, 19, 318

Marks, R. D., Vernin, J., Azouit, M., Manigault, J. F., & Clevelin, C. 1999, A&AS, 134, 161

Masciadri, E., Feldt, M., & Hippler, S. 2004, ApJ, 613, 572

Roddier, F. 1981, Prog. Opt., 19, 281

Roddier, F., Gilli, J. M., & Lund, G. 1982a, J. Optics, 13, 263

Roddier, F., Gilli, J. M., & Vernin, J. 1982b, J. Optics, 13, 63

Shao, M., & Colavita, M. M. 1992, A&A, 262, 353

Sozzetti, A. 2005, PASP, 117, 1021

Swain, M. R., Coude du Foresto, V., Fossat, E., & Vakili, F. 2003, Mem. Soc. Astron. Italiana Supp., 2, 207

Swain, M. R., et al. 2004, Proc. SPIE, 5491, 176

Tokovinin, A., Kornilov, V., Shatsky, N., & Voziakova, O. 2003, MNRAS, 343, 891

Tokovinin, A., & Travouillon, T. 2006, MNRAS, 365, 1235

Tokovinin, A., Vernin, J., Ziad, A., & Chun, M. 2005, PASP, 117, 395

Travouillon, T. 2005, in Dome C Astronomy and Astrophysics Meeting, ed. M. Giard, F. Casoli, & F. Paletou (Les Ulis: EDP Sci.), 31

Vakili, F., et al. 2004, Proc. SPIE, 5491, 1580

Walden, V. P., Town, M. S., Halter, B., & Storey, J. W. V. 2005, PASP, 117, 300

Yura, H. T., & McKinley, W. G. 1983, Appl. Opt., 22, 3353